Rearrangement and elimination of ordered surface layers of crystalline bubble structures due to gas diffusion

Antje van der Net,* Denis Weaire and Stefan Hutzler

Received 30th May 2008, Accepted 18th August 2008
First published as an Advance Article on the web 21st November 2008
DOI: 10.1039/b809169b

We describe a hitherto unknown self-organising effect in wet crystalline bubble structures exposed to air. Due to the escape of gas from the bubbles in the top surface layer, bubbles shrink and create space for the bubbles of the lower layers to interpose themselves at the top. This occurs irregularly, but finally a newly ordered bidisperse top layer is formed. This process can be followed for several episodes of elimination of surface layers. The crystalline orientation influences the speed of shrinkage and formation of the bidisperse top layer. Compared with diffusion of a single bubble or monodisperse monolayer on top of a liquid pool, the diffusion is much faster. This may be accounted for by the extra buoyancy force leading to a larger exposure of the bubbles at the surface.

1 Introduction

Foams have a finite lifetime. They coarsen due to the effect of coalescence and diffusion. Foam films break if they become too thin due to drainage.[1,2] Diffusion occurs as gas migrates *via* the films from one bubble to another, from high to low gas pressures, resulting in shrinkage of smaller bubbles, while larger bubbles grow.

Previous coarsening studies focused on dry foams, especially in two dimensions.[3] Current investigations study dry and wet foams in three dimensions using imaging techniques such as diffusive light spectroscopy,[4,5] magnetic resonance imaging,[6] X-ray tomography[7,8] or optical tomography.[9] The main focus of interest is the behaviour of bubbles in the bulk,[10] boundary effects occurring at the foam–atmosphere interface are generally not considered.

The work presented here deviates from this approach by concentrating solely on the behaviour of bubbles at this interface. In particular we study the top layer of crystalline microfoams of equal-sized bubbles with values of liquid fractions larger than twenty percent.[11–13] While initially diffusion leads to loss of order in the top layer, eventually order is re-established, but now in the form of a bidisperse top layer which appears within 5–10 min. As the smaller bubbles disappear this effect repeats itself. We will describe the process in more detail for the different crystalline structures and surfaces of fcc (100) and fcc (111)/hcp oriented crystals.

We also find that the diffusion of the top layer of the bubble crystals is faster (within 10 min) than that for single bubbles or monolayers (2 h), and that it increases in a roughly linear manner with the number of bubble layers in the foam. (All our bubbles had initial diameters between 190 and 380 μm.)

2 Experiment and analysis

We performed experiments on the gas diffusion associated with single bubbles, monodisperse layers and different crystalline structures of bubbles, floating on a liquid. We used an aqueous solution with 1% volume fraction of the commercial detergent Fairy liquid (the concentration is 10 times higher than the CMC, with a surface tension of 28 mN m^{-1}), which is known to give stable foams.

Equal-sized single bubbles were generated either using the microdispenser,[14] a special device which allows controlled release of discrete volumes of *air* through a needle (200 μm in diameter) into a liquid, or by the use of a microfluidic flow focusing device for large production of bubbles filled with *nitrogen*. The flow focusing device is based on continuously focusing gas and liquid through a small orifice (∼ 400 μm), thereby creating a jet of gas which becomes unstable and breaks up into monodisperse bubbles.[15,16,17,18] The production is up to 200 bubbles s^{-1} and we can achieve diameters within the range of 100–700 μm, using different ratios of flow rates of gas and liquid. For the creation of monolayers or the crystalline bubble structures consisting of up to 23 layers on top of a liquid surface we only used the flow focusing device, *i.e.* all these structures contained bubbles filled with nitrogen. Depending on the quantity deposited, the bubbles either form a single monolayer, arranged in a close-packed triangular pattern,[19] or spontaneously crystallise in fcc (111) or hcp and fcc (100) bulk structures[11,12] with a triangular or square-ordered surface layer, respectively. In the following we will refer to these ordered three-dimensional bubble arrangements as 'bubble crystals'. The liquid volume fraction in these crystals exceeds 20%,[12] thus the bubbles remain nearly spherical.

A liquid pool containing the bubble(s) was placed on an overhead projector in order to visualize the bubble(s) with transmitted light. Using a digital camera (Nikon Coolpix 4500) attached to a microscope, images were taken at regular intervals (5 min for bubbles and monolayers and 1 min for bubble crystals). The data was analysed with the image processing software ImageJ[20] to obtain bubble size distributions as a function of time. A correction factor was applied to account for the 10% underestimation of the bubble radii due to the details of the light propagation in a bubble.[21]

The heat generated by the overhead projector leads to a gradual increase in the water temperature. Increasing temperatures should lead to an increase in gas permeability of soap

School of Physics, Trinity College Dublin, Dublin 2, Ireland. E-mail: vanderna@tcd.ie; dweaire@tcd.ie; shutzler@tcd.ie

films,[22] thus to a faster shrinkage of the bubbles. The small temperature difference of 2–3 °C between the beginning and end of our experiments might thus contribute to the uncertainty of our measurements of the permeability.

As mentioned earlier, the diffusion rate of the top layer depends on the number n of bubble layers in foam, whose precise value is, however, not easy to determine. Here we proceeded by measuring the local foam thickness h, defined as the difference in height between the foam–air and foam–water interface at the beginning of the experiment, and dividing it by the layer thickness for the observed local structure, *i.e.* $h = (n-1)*\sqrt{2}R_0 + 2R_0$ for fcc (111) or hcp (both have a triangular top layer), or $h = (n-1)*\sqrt{8/3}R_0 + 2R_0$ for fcc (100) with its square-ordered top layer. Here R_0 is the initial bubble radius measured at the start of the experiment. For multi-layer foams it is not obvious that a particular type of bubble rearrangement is maintained throughout a section of sample, also the measurement of the thickness includes inaccuracies. Based on this we attach an error of ± two layers to local thicknesses exceeding 5 layers.

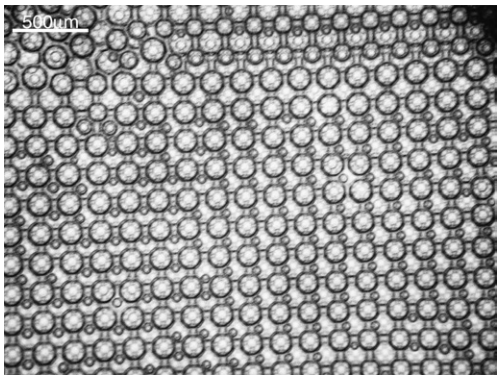

Fig. 1 A bidisperse top layer of an fcc (100) oriented bubble crystal.

3 The creation of bidisperse top layers

In this section we describe the occurrence of bidisperse top layers in crystals oriented in fcc (100) and fcc (111), of the former an example is shown in Fig. 1, showing bubbles in the top layer with two different diameters. Further we discuss how diffusion results in the elimination of successive layers of the crystal.

Fig. 2 shows a sequence of images of a fcc (100) oriented surface. At the start of the observation the bubbles are approximately monodisperse (within a standard deviation of 2%) and are arranged in a square lattice. As they shrink and lose contact with their neighbours, bubbles from the layers below begin to interpose themselves into the top layer, driven by buoyancy. The foam–gas interface will slightly drop as the top layers of bubbles begin to shrink. With respect to the level of the top layer the larger bubbles of the second layer rise up as space has been created at the interface.

Initially the intrusion of bubbles from the second layer happens somewhat randomly, leading to the creation of a new disordered top layer, with some bubbles from the second layer and the smaller initial top layer present. Possibly slight polydispersity in the bubble sizes plays a role in the randomness of the position where new bubbles appear at the surface. Nevertheless, eventually the bubbles of the original top layer fit into the gaps of the second layer, now completely moved upwards, and together

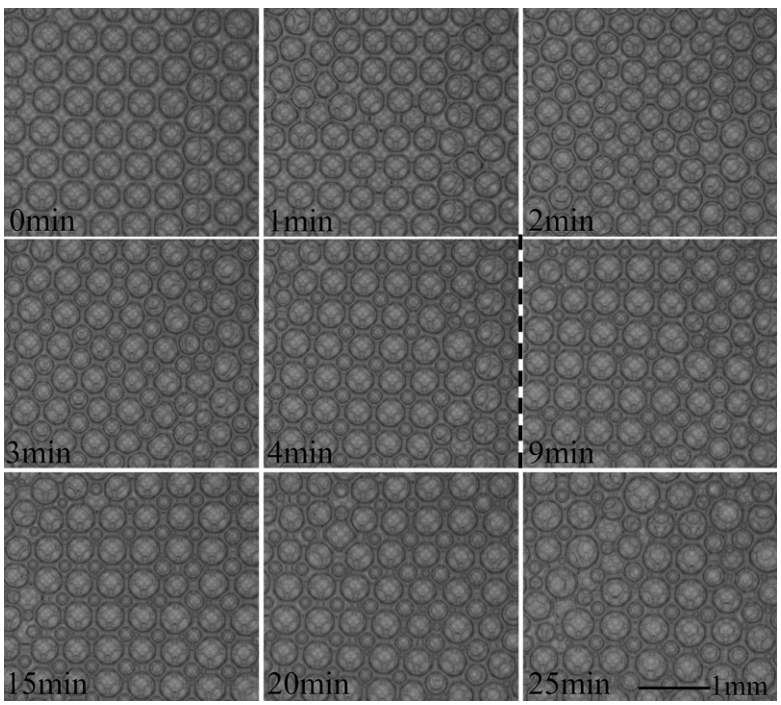

Fig. 2 The effect of diffusion in an fcc (100) oriented crystalline bubble structure. Here $t = 0$ marks the completion of deposition of the bubbles onto the water surface. After 4 min a bidisperse top layer is formed by the first and second layer of the crystal. This process repeats itself every five minutes, with the bidisperse layers being formed from two successive layers. After 25 min defects start to play a large role and the top layer becomes disordered.

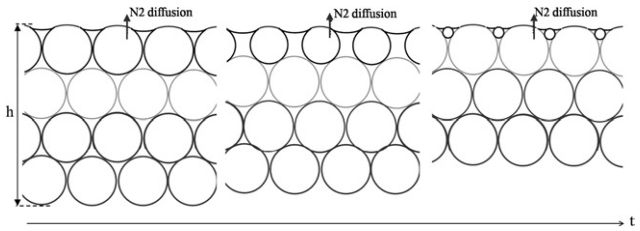

Fig. 3 A cross-section through the bubble crystal, showing a sketch of the diffusion process in time. (h is the initial height of the foam.)

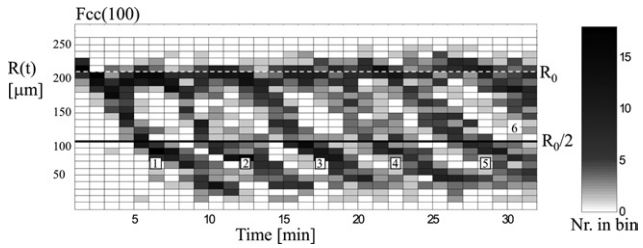

Fig. 4 Sequence of diffusion data for the square fcc (100) oriented crystalline bubble structure of Fig. 2. The graph shows for each minute the radial size distribution $R(t)$ of the bubbles. The gray scale represents the number of bubbles within a range of bubble sizes. The numbers label the different layers that rise to the top during the diffusion. R_0 is the average initial bubble radius before diffusion sets in. Bidispersity approximately occurs at $R(t) = R_0/2$.

they form a perfectly *ordered* bidisperse top layer, as sketched in Fig. 3.

Following the diffusion further in time we find that the same effect repeats itself. The new top layer proceeds to shrink, disorder and re-order in the same way. We were able to follow the bidisperse surface formation up to the elimination of the fifth layer. At that stage defects, disorder induced at boundaries between grains of different crystalline structures and internal coarsening start to play a large role and diffusion no longer results in ordered bidisperse surface layers.

Fig. 4 (a) shows the temporal evolution of histograms of bubble radii, obtained from a comprehensive image analysis of the top layer. A periodic pattern can be seen, where each branch represents the elimination of a layer, numbered 1–6. It can be seen that initially there is already a difference in sizes, caused by diffusion occurring before the imaging started; this speeds up in the next 3–4 min. After 4 min a separation is clearly visible in the size distribution and layer 2 appears at the top surface. At this stage, with bubble radius R smaller than 100–150 μm, the diffusion of layer 1 slows down and the small bubbles remain present even after the third layer (3) appears at the surface and forms with second layer (2) a bidisperse top layer again. Three generations of bubbles are then present. The bubbles of the initial top layer (1) are randomly distributed and do not influence the ordering of the next layers. After 10 min they have disappeared. This process repeats itself up to 6 layers. Generally a new layer appears every 5–6 min and remains present for about 10 min. Note that the initial bubble radius of the appearing layer

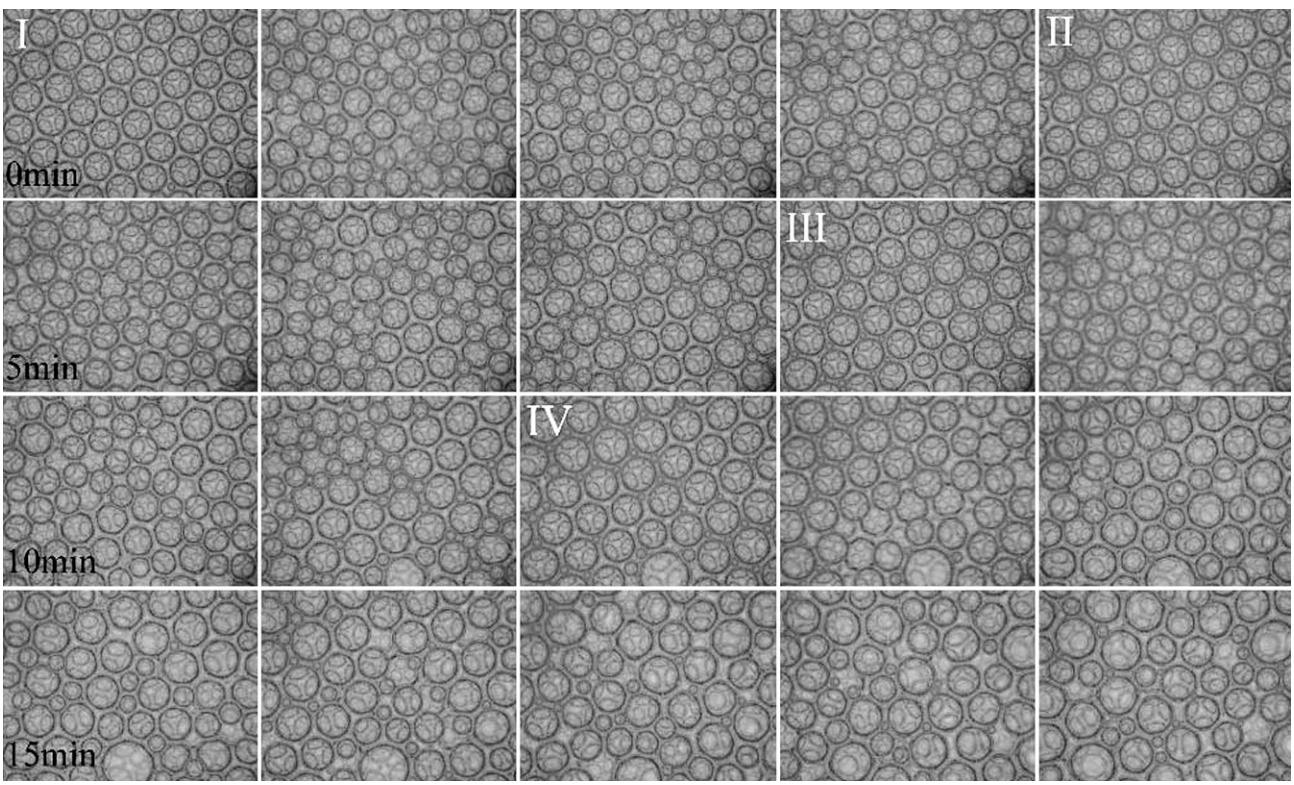

Fig. 5 The process of diffusion of a triangular oriented crystalline bubble structure. One picture is made per minute, where $t = 0$ marks the end of the deposition of the bubbles onto the water surface. The sequence shows the appearance of new layers labeled II to IV, indicated in Fig. 6.

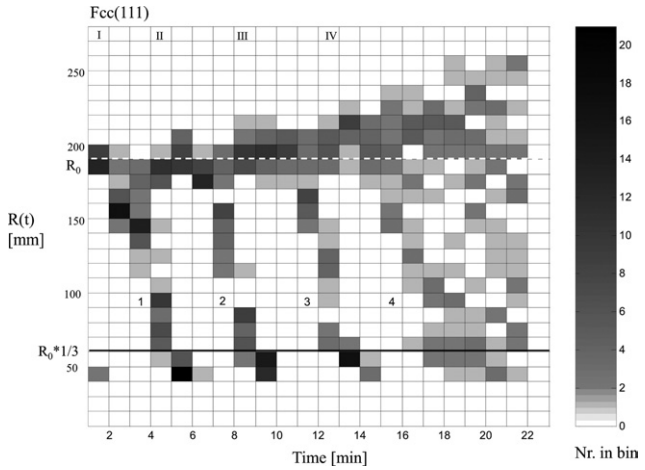

Fig. 6 The process of diffusion of a triangular oriented crystalline bubble structure. The labels I to IV correspond to the labelled images in Fig. 5. The numbers 1 to 4 label the different layers. The graph shows for each minute the radial size distribution $R(t)$ of the bubbles. The gray scale represents the number of bubbles within a range of bubble sizes. The numbers label the different layers that rise to the top during the diffusion. R_0 is the average initial bubble radius before diffusion sets in. Completion of bidispersity approximately occurs at $R(t) = R_0/3$. (Note that the increase in the radius of the bubbles in the top layer, and the spread in size, indicates that these bubbles have started to coarsen in the bulk, before they arrive at the top.)

increases. This can be caused either by diffusion between the bubbles of the two top layers or by internal coarsening.

In Fig. 5 and 6 the effect of gas diffusion is shown for a triangular fcc (111) surface. Again space is created for the bubbles of the second layer (2) to squeeze towards the gas–water interface. Eventually the second layer is completed, again forming a bidisperse layer but this time the bubbles of the initial surface layer are much smaller than in the bidisperse top layers of fcc (100), as can be seen in Fig. 7. As for these triangular oriented surfaces there are twice as many holes to fill than there are bubbles present in one layer, these do not form a perfectly filled ordered bidisperse top layer.

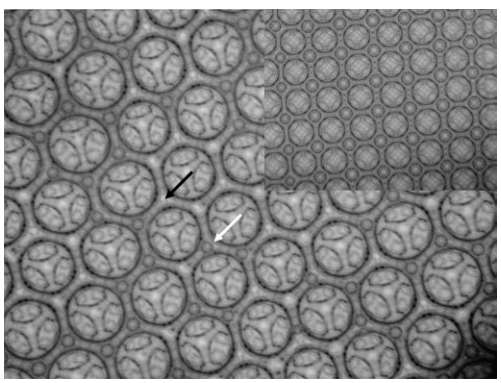

Fig. 7 The incomplete bidisperse top layer of fcc (111) compared with the complete fcc (100) (inset). The black arrow points to an empty cavity, the white arrow shows a small bubble, which is a remnant of the initial top layer.

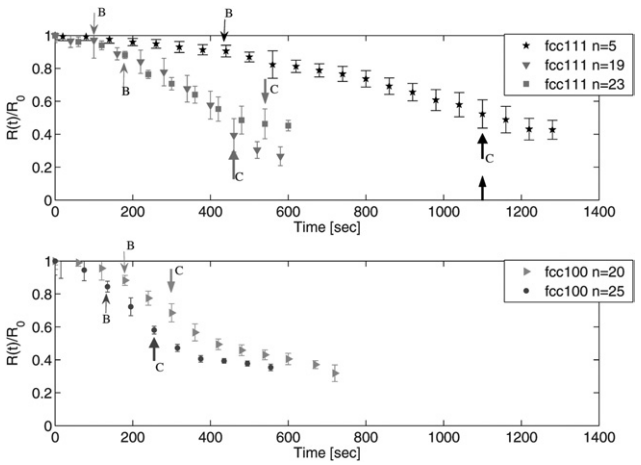

Fig. 8 Time evolution of bubble radii in crystals with either triangular top layers (top) or square top layers (bottom). The arrows labeled B mark the appearance of the first bubbles of the second layer and the arrows labeled C mark the first occurrence of the visible bidisperse top layer.

In due course the third layer (3) starts to appear. At this stage the initial top layer has completely disappeared. This process of layer replacement could be followed up to 4 layers.

We are interested how, for a particular bubble crystal with a fixed number of layers, the average bubble radius of the top layer varies with time. In Fig. 8 we have normalised $R(t)$ by the average initial bubble radius R_0 at the start of each experiment, for both triangular and square oriented crystals. We have marked the appearance of the first bubbles of the second layer (B) and the completion of the bidisperse top layer (C). We will look in more detail at the initial stage of diffusion (before the appearance of bubbles from layer 2) where all surface bubbles shrink at the same rate in the following section.

Occasionally we have observed a different mechanism for the emergence of the second layer, as can be seen in Fig. 9. The surface layer splits open along a row of bubbles and a row from the second layer appears at the top surface (marked by arrows). This is seen more often near ordered grain boundaries or stacking faults.

4 Diffusion rate

From Fig. 8 it is obvious that the shrinkage rate of bubbles in the top layer of bubbles increases with the number of layers in the crystal. In this section we describe how we apply an existing theoretical model to describe the diffusion of a single bubble on a liquid pool to our bubble crystals to quantify the diffusion rate dependence on the amount of layers present. Therefore we also conducted experiments with both individual bubbles and monolayers of equal-sized bubbles sitting on a pool of liquid. Fig. 10 shows all our data gathered. Single bubbles and monolayers exist for up to 10 000 s while the lifetime of bubbles in the top layer of our crystals is less than 2000 s.

We use the model of Ghosh and Juvekar,[22] who measured and modeled the effect of temperature on the permeability of films of bubbles at the liquid–gas interface. This model describes the volume change of a bubble being dependent on the atmospheric pressure, the gas pressure difference across the film, the film area

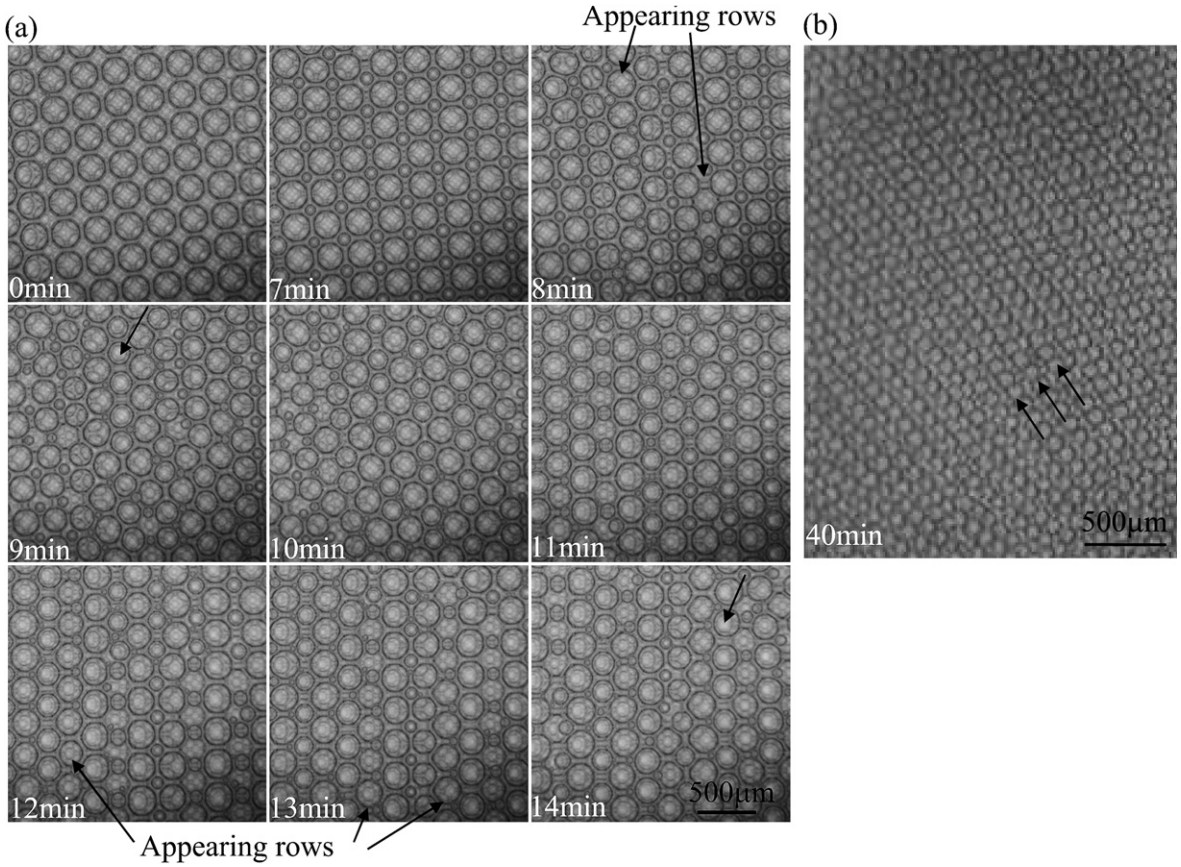

Fig. 9 (a) An alternative mode of diffusion for fcc (100). The top surface splits open along a row, allowing new rows from the second layer to intrude. In this case no bidisperse surface layers are created. This type of crystalline diffusion maintains ordered rows of bubbles for as long as 40 min, see (b), *i.e.* nearly twice as long as is the case for the type of diffusion in Fig. 2 and 5. Arrows in (b) indicate three of them.

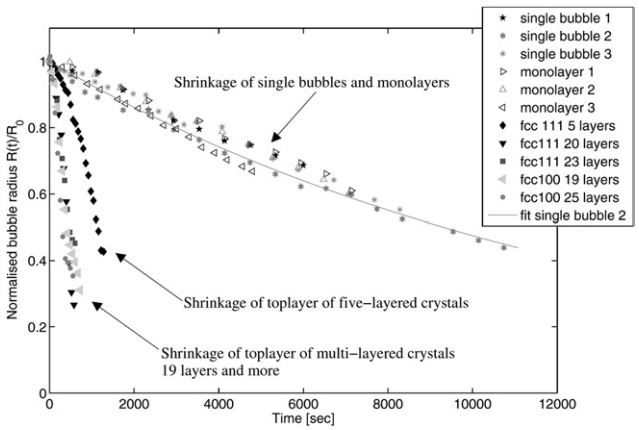

Fig. 10 The bubble size reduction in time for different configurations of bubbles at a liquid surface. The shrinkage of the top layers of bubbles in crystals is much quicker than for bubbles in a monolayer or for a single layer.

and the film permeability k. This results in an equation relating time of diffusion t to the decrease in bubble radius $R(t)$:

$$t = t_0 + \frac{U}{k} * \left[\sqrt{1-B} - \sqrt{1-CR(t)^2} + \ln \frac{1-\sqrt{1-B}}{1-\sqrt{1-CR(t)^2}} \right] \quad (1)$$

with

$$U = \frac{3P}{4\Delta\rho g}$$

$$B = \frac{R_0^2 \Delta\rho g}{3\gamma}$$

$$C = \frac{\Delta\rho g}{3\gamma}$$

with R_0 as the initial bubble radius measured at $t = t_0$, P the atmospheric pressure, $\Delta\rho$ the density difference between the gas and liquid, g the gravitational acceleration constant and γ the surface tension. Applying the model to our data for the single bubble and monolayers of bubbles we determined the rate of diffusion of gas (m s^{-1}), the *permeability*, k, through the top film. We fitted each data set of t *versus* $R(t)$ to this equation using the least square fitting routine in Gnuplot with the permeability as the free fitting parameter. Since the data for single bubbles and monolayers overlap we conclude that initially the diffusion between the bubbles within the layer is negligible, resulting in an average estimated permeability of $1.11 \pm 0.15 \times 10^{-3}$ m s^{-1} for a film stabilised by a Fairy liquid surfactant concentration of 1 volume% at 18–21 °C. The value seems reasonable compared with published film permeabilities, as shown in Table 1. Note

Table 1 The permeabilities obtained for our five experiments performed with single bubbles floating at a liquid surface and three experiments performed with monolayers of bubbles floating at the liquid surface. These values are comparable with similar values found in the literature

			R_0/μm	k/m s^{-1}	T/°C	Surfactant
Experiment	1	Single bubble	370	$0.98 \pm 0.02 \times 10^{-3}$ (air)	21–22	Fairy
	2	Single bubble	380	$1.19 \pm 0.01 \times 10^{-3}$ (air)	22	Fairy
	3	Single bubble	350	$1.05 \pm 0.02 \times 10^{-3}$ (air)	18–21	Fairy
	4	Single bubble	330	$0.97 \pm 0.02 \times 10^{-3}$ (air)	20	Fairy
	5	Single bubble	520	$1.21 \pm 0.04 \times 10^{-3}$ (N_2)	20	Fairy
	1	Monolayer	240	$1.02 \pm 0.03 \times 10^{-3}$ (N_2)	18–21	Fairy
	2	Monolayer	190	$0.98 \pm 0.02 \times 10^{-3}$ (N_2)	20–21	Fairy
	3	Monolayer	250	$1.26 \pm 0.02 \times 10^{-3}$ (N_2)	18–19	Fairy
Literature		Princen and Mason[23,24]	133.6–376.0	1.23×10^{-3} (air)	21	Hexadecyltrimethylammonium
		Krustev *et al.*[25]	Liquid film	$0.3 - 1 \times 10^{-3}$ (air)	21–30	SDS–NaCl
		Krustev *et al.*[26]	Liquid film	$0.85 - 1.65 \times 10^{-3}$ (air)	25	SDS–LiCl
		Muruganathan *et al.*[27]	Liquid film	$1.25 \pm 0.02 \times 10^{-3}$ (air)	25	Dodecyl maltoside–NaCl

that in the model of Ghosh and Juvekar[22] it is assumed that the gas concentrations are constant at either side of the film. Our bubble crystals are filled with nitrogen but diffuse effectively towards air. Comparing permeability estimations of nitrogen or air filled bubbles, the accuracy of the experiment is not large enough to distinguish between the two cases. So this allows us to use the model with nitrogen filled bubbles diffusing towards the atmosphere.

The scatter present in our data is possibly due to variable environmental factors, *e.g.* temperature during the experiment, of air and liquid. Increasing temperatures can increase the diffusion rate.[22,26] Other factors can be slight polydispersity of the initial bubbles, errors in the image analysis due to the picture quality (due to bubble movement) and optical effects.

Having established a value for k we have applied the model to the diffusion data of the top layer bubbles in the regime where top layer bubbles are monodisperse and no bubbles from the second layers are present yet. At this initial stage of the experiment the radii decrease approximately linearly with time, as is shown in Fig. 11, and the magnitude of the slopes increases with the number of bubble layers. We can thus linearise eqn (1) to get:

$$t - t_0 = 1 - \frac{3P}{2k\Delta\rho g}\left[\frac{R(t)}{R_0}\right] \tag{2}$$

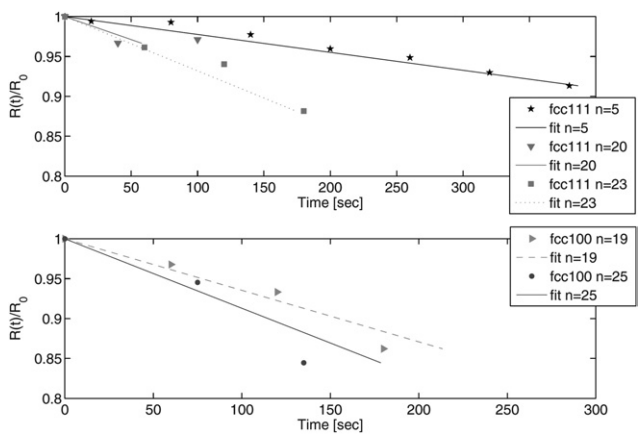

Fig. 11 A zoom in on Fig. 8. At the initial stage of bubble shrinkage in the top layer, the bubble radii vary approximately linear with time. Eqn (2) is fitted to this data.

For a single bubble, or single layer, the slope is thus given by $-\frac{3P}{2k\Delta\rho g}$. To account for the effect of multiple layers underneath the top layer of bubbles we added an extra factor β in eqn (1), which effectively increases the buoyancy (see the Discussion for possible interpretations of this factor), resulting in:

$$t - t_0 = 1 - \frac{3P}{2k\Delta\rho g\beta}\left[\frac{R(t)}{R_0}\right] \tag{3}$$

In the least square fits of our data to eqn (2) we have used the value of k that we determined from our earlier measurements and used β as our free parameter. Its variation with the amount of layers is shown in Fig. 12. β increases almost linear with the increasing number of layers n, according to $\beta = 0.41n + 0.68$. In this analysis no distinction is made between the different crystalline structures.

5 Discussion

While it takes hours for a single bubble to disappear due to diffusion, bubbles in a top layer of a bubble crystal disappear roughly after a few minutes. Different aspects of the system can

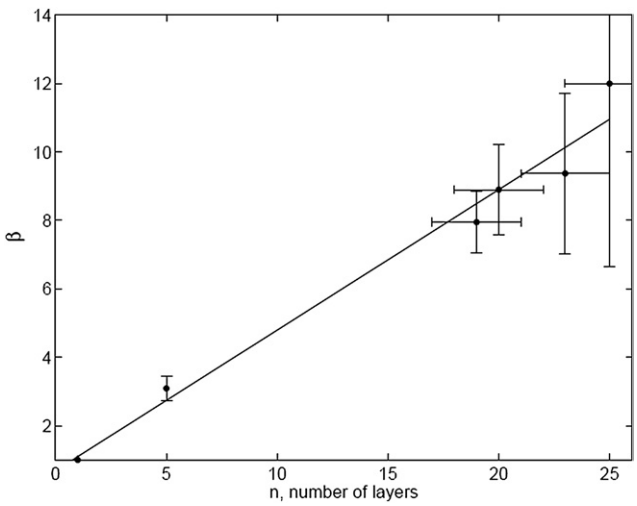

Fig. 12 Variation of the fit parameter β of eqn (2), with the number of layers in the bubble crystal. β may be interpreted as representing a buoyancy multiplier.

contribute to this effect and are thus responsible for the variation of β, as shown in Fig. 3.

An extra buoyancy force from the extra layers below, pushing the top layer up, resulting in an increase in the area of diffusion could be one of the factors. To theoretically describe the role of the extra buoyancy force on the top layer bubbles would require an actual definition of buoyancy forces of bubbles in a foam.

The foam becomes dryer at the top when more layers are present. This change in liquid fraction of the top layer can play a role, in two ways. When the top layer becomes dryer the exposed cap area can increase, as well as film permeabilities. More experimental data is needed to include/exclude this effect. It would be of interest as well to explore the variation of β with more than 25 layers. The same experimental procedure for top-layer diffusion can be applied to samples with more than 25 layers. Monitoring of the bubble size nevertheless will become more difficult as the bubbles are more polyhedrally shaped and the surface patterns, as are present for spherical bubbles, will be less clear. β is expected to level off such that it becomes independent of the amount of layers.

So far we only quantitatively studied the *initial* stage of the top layer diffusion with no bubbles of the second layer present. As can be seen in Fig. 8 after the first bubbles of the second layer appear (B) the bubble shrinkage speeds up. This could be caused by the extra diffusion taking place between the surface bubbles of different sizes. With some delay after complete appearance of the second layer at the surface forming a bidisperse top layer (C), bubble shrinkage of the initial top layer bubbles decreases significantly. Possibly the bubbles are so small at this stage that they loose contact with the surrounding bubbles and can be considered as a single floating bubble again. These two later stages need further investigation in the future.

6 Conclusion and outlook

In this article we studied the boundary effect on ordered bulk foams and diffusion of top layers of ordered bubble crystals. Surprisingly the diffusion self-organises the top layers after a disordered stage into bidisperse top layers, which is repeated and can be followed for several iterations. The reason for the re-occurrence of order is not yet understood.

In the future experimental permeability data needs to be generated on the variation of permeability with film thickness, for example by the method proposed by Krustev and Müller.[28] More knowledge needs to be gained on buoyancy effects in foams in order to completely understand the observed effects. This will be of fundamental interest. It would be interesting to study the effects of different gases and surfactants on the diffusion process.

The progressive elimination of surface layers peels off the exposed surface. Following the ordered coarsening of up to 6 layers is thus another indication, in addition to the mentioned optical patterns and terraces, that the bulk structure is ordered.[12] This effect may be used in the future to study the arrangement of dislocations, or other layer defects, although dislocations can initiate different coarsening rates.

In general, this diffusion effect obstructs the ability to use bubble crystals exposed to air, and needs to be avoided but on its own it presents another unique property of bubble crystals.

7 Acknowledgements

We would like to thanks C. Stubenrauch and R. Krustev for discussions of film permeability. V. Carrier and V. Langlois are thanked, respectively, for discussions of the liquid fraction in foams and the comparison with granular materials. This work was supported by Science Foundation Ireland (RFP 05/RFP/PHY0016), the European Space agency ESA (contracts 14914/02/NL/SH and 14308/00/NL/SH) and COST (European Science Foundation) P21, The Physics of Droplets.

References

1 A. Saint-Jalmes and D. Langevin, *J. Phys.: Condens. Matter*, 2002, **14**(40), 9397–9412.
2 M. U. Vera and D. J. Durian, *Physical Review Letters*, 2002, **88**(8), 088304.
3 D. Weaire and S. Hutzler, *The Physics of Foams*, Clarendon press, Oxford, 1999.
4 D. J. Durian, D. A. Weitz and D. J. Pine, *J. Phys.: Condens. Matter*, 1990, **2**, SA433–SA436.
5 D. J. Durian, D. A. Weitz and D. J. Pine, *Phys. Rev. A*, 1991, **44**(12), R7902–R7905.
6 C. P. Gonatas, J. S. Leigh, A. G. Yodh, J. A. Glazier and B. Prause, *Phys. Rev. Lett.*, 1995, **75**(3), 573–576.
7 J. Lambert, I. Cantat, R. Delannay, A. Renault, F. Graner, J. A. Glazier, I. Veretennikov and P. Cloetens, *Colloids Surf., A: Physicochemical and Engineering Aspects*, 2005, **263**(1–3), 295–302.
8 J. Lambert, I. Cantat, R. Delannay, R. Mokso, P. Cloetens, J. A. Glazier and F. Graner, *Phys. Rev. Lett.*, 2007, **99**(5), 058304.
9 C. Monnereau and M. Vignes-Adler, *Phys. Rev. Lett.*, 1998, **80**(23), 5228–5231.
10 A. M. Ganan-Calvo, J. M. Fernandez, A. Marquez Oliver and M. Marquez, *Appl. Phys. Lett.*, 2004, **84**(24), 4989–4991.
11 L. Bragg and J. F. Nye, *Proc. R. Soc. London, Ser. A: Mathematical and Physical Sciences*, 1947, **190**(1023), 474–481.
12 A. van der Net, W. Drenckhan, D. Weaire and S. Hutzler, *Soft Matter*, 2006, **2**(2), 129–134.
13 A. van der Net, W. Drenckhan, G. W. Delaney, D. Weaire and S. Hutzler, *Colloids Surf. A: Physicochemical and Engineering Aspects*, 2007, **309**, 117–124.
14 DeeracFluidics (www.deerac.com), microdispenser.
15 C. S. Smith, *J. Appl. Phys.*, 1949, **20**(6), 631–631.
16 J. M. Gordillo, Z. Cheng, A. M. Ganan-Calvo, M. Marquez and D. A. Weitz, *Phys. Fluids*, 2004, **16**(8), 2828–2834.
17 I. Cohen, H. Li, J. Hougland, M. Mrksich and S. R. Nagel, *Science*, 2001, **292**, 265–267.
18 A. S. Utada, E. Lorenceau, D. R. Link, P. D. Kaplan, H. A. Stone and D. A. Weitz, *Science*, 2005, **308**(5721), 537–541.
19 M. M. Nicolson, *Proc. Cambridge Philos. Soc.*, 1949, **45**(2), 288–295.
20 ImageJ: http://rsb.info.nih.gov/ij/.
21 A. van der Net, L. Blondel, A. Saugey and W. Drenckhan, *Colloids Surf. A: Physicochemical and Engineering Aspects*, 2007, **309**, 159–176.
22 P. Ghosh and V. A. Juvekar, *J. Chem. Eng. Jpn.*, 2003, **36**(6), 711–715.
23 H. M. Princen and S. G. Mason, *J. Colloid Sci.*, 1965, **20**, 353–375.
24 H. M. Princen and S. G. Mason, *J. Colloid Sci.*, 1965, **29**, 156–172.
25 R. Krustev, D. Platikanov and M. Nedyalkov, *Colloids Surf. A: Physicochemical and Engineering Aspects*, 1993, **79**(1), 129–136.
26 R. Krustev, D. Platikanov and M. Nedyalkov, *Colloids Surf. A: Physicochemical and Engineering Aspects*, 1997, **123**, 383–390.
27 R. M. Muruganathan, R. Krustev, H. J. Muller, H. Mohwald, B. Kolaric and R. von Klitzing, *Langmuir*, 2004, **20**(15), 6352–6358.
28 R. Krustev and H. J. Muller, *Rev. Sci. Instrum.*, 2002, **73**(2), 398–403.

